Journal of Hazardous Materials 423 (2022) 127197

Contents lists available at ScienceDirect

Journal of Hazardous Materials

journal homepage: www.elsevier.com/locate/jhazmat

Pivotal role of water molecules in the photodegradation of pymetrozine: New insights for developing green pesticides

Ximei Liang [a,1], Fangling Guan [b,1], Zhiyou Ling [b], Honghong Wang [c], Yunwen Tao [d], Elfi Kraka [d], Huajun Huang [b], Chenglong Yu [b], Danping Li [b], Jinbao He [b], Hansun Fang [b,*]

[a] College of Animal Science and Technology, Jiangxi Agricultural University, Nanchang 330045, China
[b] Key Laboratory of Poyang Lake Basin Agricultural Resource and Ecology of Jiangxi Province, College of Land Resource and Environment, Jiangxi Agricultural University, Nanchang 330045, China
[c] State Key Joint Laboratory of Environment Simulation and Pollution Control, Research Center for Eco-Environmental Sciences, Chinese Academy of Sciences, Beijing 100085, China
[d] Department of Chemistry, Southern Methodist University, 3215 Daniel Ave, Dallas, TX 75275-0314, USA

ARTICLE INFO

Editor: Dr. L. Angela Yu-Chen

Keywords:
Photodegradation
Water molecules
Photoinduced hydrolysis
Pymetrozine
Mechanism

ABSTRACT

Photodegradation of the insecticide pymetrozine (PYM) was studied on surface of wax films, and in aqueous and nonaqueous phase. The half-life of PYM on the wax surface was approximately 250 times longer than in water. Scavenging experiments, laser flash photolysis, and spectra analysis indicated the first singlet excited state of PYM (S1 $^{*}_{PYM}$) to be the most important photoinduced species initiating the photodegradation. Quantum chemistry calculations identified significant molecular torsion and changes in the structure C–C═N–N of S1 $^{*}_{PYM}$, and the absolute charges of the C═N atoms increased and the bond strength weakened. Free energy surface analysis, and O^{18} labeling experiments further confirmed that the mechanism was two-step photoinduced hydrolysis. The first step is the hydrolysis of S1 $^{*}_{PYM}$ at C═N upon reaction with 2–3 water molecules (one H_2O molecule as the catalyst). The second step is an intramolecular hydrogen transfer coupled with the cleavage of C–N bond and formation of two cyclic products. During the interactions, water molecules experience catalytic activation by transferring protons, while there is a negligible solvent effect. Clarifying the detailed photodegradation mechanisms of PYM is beneficial for the development of green pesticides that are photostable and effective on leaf surfaces, and photolabile and detoxified in the aquatic environment.

1. Introduction

The annual usage of pesticides continues to increase at the global scale, in particular, in developing countries. Some recent estimates indicate the amount might have surpassed 3.47 million tons in 2020 (Sharma et al., 2019; Zhang, 2018). Many pesticides are primarily sprayed on the leaf surfaces of crops, including pesticides that target foliar-feeding insects, foliar fungi, and diseases that require chemicals to be absorbed by leaves. After usage, pesticides generally dissipate from the crop leaf surfaces through volatilization, plant uptake, wash-off, and photodegradation (Ebrahimi et al., 2013; Kah et al., 2019; Sleiman et al., 2017). During field application, pesticide loss is usually balanced by high application rates. However, pesticides can be washed off easily by rainfall (Perez-Rodriguez et al., 2017), thus high pesticide applications may result in the increased contamination of downstream aquatic systems. This can increase risks to non-target organisms (De Souza et al., 2020), and eventually threaten human health through the food chain (Kim et al., 2017; Kuang et al., 2020).

Solar light plays an important role in pesticide dissipation (Zeng and Arnold, 2013). Moreover, on environmental surfaces, such as the sun-illuminated area of a leaf, water, and soil, solar ultraviolet (UV) light is likely to depress microbial growth and metabolism (Slieman and Nicholson, 2000; Theitler et al., 2012). This indicates that photodegradation may be the major process for pesticide dissipation on the surface of specific substances (Fenner et al., 2013). In general, pesticides undergo direct and indirect photodegradation. Direct photodegradation indicates that pesticides directly absorb solar photons and get degraded through electron transfer, photoionization, and bond cleavage (Di

* Corresponding author.
E-mail address: fanghansun@163.com (H. Fang).
[1] X.M. Liang and F.L. Guan were co-first authors contribute equally to this work.

https://doi.org/10.1016/j.jhazmat.2021.127197
Received 13 May 2021; Received in revised form 4 August 2021; Accepted 8 September 2021
Available online 11 September 2021

Nunzio et al., 2009; Shkrob, 2010). In contrast, indirect photodegradation indicates that pesticides react with reactive oxygen species (ROS); examples include singlet oxygen, superoxide anion, and hydroxyl radical. These are generated by photoexcited photosensitizers in the surrounding environment (Anglada et al., 2020; Zeng and Arnold, 2013).

It is expected that significant differences in the photostability of a pesticide on a leaf surface and in an aqueous phase may highlight ways to control agricultural non-point source pollutants. First, increasing the resistance of pesticides to photodegradation on the leaf surface can decrease the usage amount and frequencies. Second, the rapid degradation of pesticides in aquatic environment would probably lower its environmental risks if the pesticides could be mineralized or decomposed into products with lower toxicity. Some studies have investigated the photodegradation of pesticides in water, and a few studies have investigated the photodegradation of pesticides on the leaf surface (Monadjemi et al., 2011; Sleiman et al., 2017). Nonetheless, simultaneous investigation and comparison of the photolytic kinetics and mechanisms of pesticides on leaf surfaces and in water have rarely been studied till date.

Pymetrozine (PYM) is a new azo base insecticide that exhibits selective activity against homopterous insects (aphids and planthoppers) and the pollen beetle (Jia et al., 2019; Satpathy et al., 2020). The annual usage of PYM was at least 4.45×10^3 t in China according to its consumption (150 g ha^{-1}) and area of rice field (2.97×10^7 ha) (National Bureau of Statistics of China, 2020; Preetha et al., 2010). PYM was detected widely in natural aquatic environment with concentrations ranging from ND to 4.8 ng L^{-1} (Casado et al., 2019; Elfikrie et al., 2020; Münze et al., 2015). However, the United States Environmental Protection Agency (EPA) has listed PYM as a "likely" human carcinogen (Zhang et al., 2007). Furthermore, several studies have found that PYM may cause mortality, reproductive interference, tissue lysis, muscle fracture, and behavioral abnormalities in non-target organisms (Broughton et al., 2014; Walker et al., 2007; Yu et al., 2018). Most studies on PYM have focused on investigating residues in crops, water, and soil (Cabizza et al., 2007; Li et al., 2011; Shen et al., 2009), revealing that the half-life of PYM was 0.7–3.5 days under the field conditions. Only one literature focused on the photodegradation kinetics of PYM in water, and reported that PYM photodegraded mainly in the direct way and exhibited an extremely short half-life of 1 h (Fang et al., 2020). Photodegradation mechanisms and pathways are generally the decisive factors that impact the photodegradation kinetics, the large variations of PYM half-lives probably indicate different photodegradation mechanisms in/on specific environmental substances. However, the detailed photolytic initiation mechanisms and degradation pathways of PYM remain unclear.

Good approaches for estimating photodegradation on the leaf surface (Monadjemi et al., 2011) include the investigation of the photodegradation of pesticide on thin wax film and in organic solvents. Therefore, using PYM as an example of a typical pesticide, this study applied experimental and computational methods to (1) investigate the photodegradation kinetics of PYM on wax film, and in water, methanol (MeOH) and pentanol (PeOH) under natural solar irradiation or by using a xenon lamp; (2) identify the photoexcitation mechanisms and role of water in initiating the photoreactions of PYM; and (3) examine the physicochemical interactions between water and PYM during the photodegradation process. This study provides basic and detailed information about the photodegradation mechanisms of PYM.

2. Materials and methods

2.1. Chemicals

Pymetrozine (PYM, purity ≥ 99%), 3-pyridinecarboxaldehyde (purity ≥ 98%), Water-^{18}O (97% ^{18}O), *p*-nitroanisole (PNA, purity ≥ 98%), pentanol (PeOH, HPLC grade), sorbic acid (*trans*, *trans*-hexadienoic acid, HAD, purity ≥ 99%), furfuryl alcohol (FFA, purity ≥ 98%), nitroblue tetrazolium chloride (NBT, purity ≥ 98%), terephthalic acid (TPA), 2-hydroxyterephthalic acid (hTPA), and wax film were obtained from Aladdin (Shanghai, China). Dichloromethane (CH_2Cl_2), acetonitrile, and methanol (MeOH, HPLC grade) were supplied by ANPEL Laboratory Technologies (Shanghai, China). All other reagents were of analytical grade and used as received without any further purification. Experimental solutions were prepared using high-purity deionized water (~18.25 MΩ cm^{-1}). The commercial product of PYM (PYM formulation) was a suspending agent containing 25% PYM in mass fraction (Kesheng Co., Ltd, Jiangsu, China).

2.2. Experiments on photodegradation kinetics

For experiments on a wax surface, a thin wax film was prepared by weighing and then melting wax (1 g) in a glass dish (diameter 3.5 cm) at 90 °C in the furnace. The wax was allowed to naturally cool down, which then formed a ~1 mm film in the dish. The mother solution was prepared by dissolving the PYM reagent or formulation in acetonitrile at concentrations of 48.11 mg L^{-1}. Thirty droplets (5 μL per droplet) of the preparations were homogeneously added dropwise on top of the wax film using a micropipette (capacity 10 μL) (Sleiman et al., 2017). The liquid droplets were arranged close to a 5 × 6 matrix on wax surface, and the acetonitrile was allowed to evaporate naturally overnight. The PYM concentration on the wax surface was found to correspond to the recommendations instructed on the package of PYM formulation (75 g ha^{-1} or 7.5 mg m^{-2}).

Experiments were performed on the roof of a building on the campus of Jiangxi Agricultural University (N 28°45'25.82", E 115°49'50.36") in August, 2019. The dishes were semi-submerged in a water bath and covered with a quartz plate to prevent dust contamination. The water temperature was maintained at 25 °C using a circulator throughout the experiment. Three dishes were collected at specific time intervals from 0 to 9 h. Films were rinsed with acetonitrile (2 mL), and 0.5 mL aliquot was withdrawn and then directly analyzed by the HPLC. Satisfactory recovery yields of PYM were achieved (91.9–98.8%) based on performing three repetitions. Alongside the entire photodegradation experiment, the photodegradation of PNA (10 μM) in a quartz tube was used to determine the variation in solar irradiance (Dulin and Mill, 1982). Control samples wrapped by aluminum foil were run concomitantly in the dark on wax surface.

The photodegradation of PYM in water and on wax surface were concurrently conducted under natural sunlight. Then, the degradation kinetics of PYM in pure water, MeOH, and PeOH were further examined when irradiated with simulated solar light (300 W xenon lamp with an AM1.5 filter; CEL-HXUV300, CEAULIGHT, Inc. Beijing, China). Three quartz tubes were placed in a double-walled cooling water jacket to keep the solutions at a constant temperature (25 °C) throughout the experiments. Specific methods for indoor experiments were based on a previous study (Fang et al., 2020). In general, all photodegradation experiments were performed in 15 mL quartz tubes containing sample (10 mL, 0.107 mg L^{-1}, under natural sunlight) or PYM (10 μM, under xenon lamp); aliquots of sample solution (0.4 mL) were collected at specific time intervals. The spectra obtained using a spectrometer (USB 2000 +; Ocean Optics Inc., USA) under actual and stimulated sunlight were compared as shown in Fig. S1. The absolute optical power of stimulated sunlight achieved at the surface of the reaction media was 2.4 kW m^{-2} (measured using a TM208 luxmeter, TENMARS, China). Moreover, the photodegradation of 10 μM PNA in quartz tube was also determined to correct the changes induced by specific geometry of the photoreaction system (e.g., the scattering and refraction of light caused by the walls of beaker and tube). The degradation kinetic constants of PYM were calculated based on Eq. (1) as follows:

$$r = d[PYM]/dt = -k'[PYM] = k[ROS][PYM] \quad (1)$$

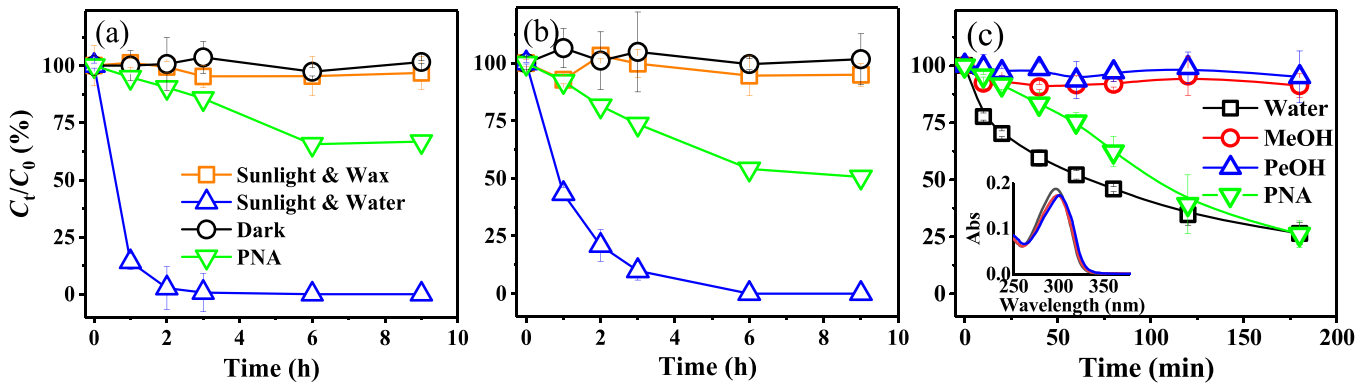

Fig. 1. The photodegradation kinetics of (a) Pure PYM reagent and (b) PYM formulation on the wax surface and in water (The level of PYM was 7.5 mg m^{-2} on wax surface and 0.107 mg L^{-1} in water). (c) The photodegradation of 10 μM PYM in water, MeOH, and PeOH under simulated solar light (inset represents the absorbance of 10 μM PYM). Photo degradation of 10 μM PNA was used for comparative analysis under the solar and lamp irradiance along with time.

where r is the degradation rate (M/s); k' is the pseudo-first-order kinetic rate constant (s^{-1}), which corresponds to the slope of the linear regression analysis of -ln(C_t/C_0) versus time (values and deviations of slope were calculated by using Origin software); k is only used in the situation of indirect photodegradation in this study, and represents the bimolecular reaction rate constant between PYM and the specific ROS (M^{-1} s^{-1}). Photodegradation half-life of PYM corresponds to ln2/k'. All photodegradation experiments were conducted in three duplicates.

2.3. Investigations of ROS

The ROS formed and involved in the photodegradation of PYM were investigated in water solution using different chemical scavengers and probes. In the scavenging experiments, a specific scavenger (1 mM) was used to remove $HO^{\bullet}$ (MeOH), $^1O_2$ (FFA), and triplet excited states (HAD and 2,4,6-trimethylphenol (TMP)). In the probing experiments, FFA (10 μM) was used to measure $^1O_2$ in a solution with 10 μM PYM. TPA (5 mM) and NBT (100 μM) were used to probe $HO^{\bullet}$ and $O_2^{\bullet-}$, respectively, in a PYM solution (50 μM).

2.4. Laser flash photolysis

Laser flash photolysis (LFP) was used to study the mechanism involved in initiating photodegradation. It was conducted using a LKS80 LFP system (Applied Photophysics Ltd., the United Kingdom). The fourth harmonic mode of the Nd:YAG laser was used; and a 266 nm laser pulse with a duration of 5 ns was used at an energy level of 10–15 mJ per pulse. A xenon lamp (150 W) was used as the detecting light source. The laser and analyzing light beam were allowed to pass perpendicularly through a 1 mm × 10 mm slit and then into a 10 mm × 10 mm × 40 mm quartz cell for the reaction. The variations in the optical signal were recorded using a Philips PM3323B digital oscilloscope; the data were output to a computer system (Lei et al., 2019). In all experiments, 80 μM PYM was used to study the transient spectra. All measurements were obtained at room temperature (25 ± 2 °C) immediately after sample preparation. An anaerobic condition was achieved by degassing the sample with high-purity N_2.

2.5. Analysis of degradation products

Gas chromatography/mass spectroscopy (Agilent 7890 GC connected to 5975 MSD, USA) was used to identify the mass spectra of degradation products. First, PYM sample (10 mL, 540 μM) was photolyzed for 8 h using the xenon lamp. The solution was extracted three times with CH_2Cl_2 (10 mL), separately. Then, the extracted samples were combined to obtain a 30 mL sample of CH_2Cl_2. The combined sample was dehydrated with Na_2SO_4, and concentrated to 1 mL by gently blowing it with N_2.

The samples for analyzing the isotopic isomers of the degradation products were obtained by photolyzing PYM (50 μM) in water-O^{16} and water-O^{18} for 4 h using the xenon lamp. The aqueous samples were directly analyzed by HPLC/MS (Agilent 1260 LC connected to 6120 MS, USA) without further treatment, and an Agilent C18 column (4.6 mm × 150 mm, 5 μm particle diameter) was used for chromatographic separations at 30 °C. The flow rate was 0.8 mL min^{-1}, and 50% acetonitrile and 50% formic acid solution (0.1%) was used as the mobile phase. The formation of isotopic isomers of 3-pyridinecarboxaldehyde was analyzed using the ESI+ mode at $m/z = 108$ and $m/z = 110$.

2.6. Calculation method

All quantum chemical calculations were conducted by using the Gaussian 16 package (Frisch et al., 2016). Geometry optimization of the first singlet excited states of PYM (S1 $^*_{PYM}$), reactants, products, and transition states (TS), and the calculations of the Gibbs free energy at 298 K were performed by using the hybrid density functional B3LYP method with a 6–311+G(d,p) basis set (Andersson and Uvdal, 2005; Becke, 1993; Lee et al., 1988). Owing to the significant geometrical variation of photoexcited PYM, optimization of TS for interactions between H_2O and PYM was based on the structure of S1 $^*_{PYM}$. The UV/Vis spectra were further calculated at the PBE0/def2-TZVPP level (nstates=20), based on the optimized structures. Intrinsic reaction coordinate theory was used to confirm that each TS accurately connected the reactant with the associated product. In all the calculations the influence of the solvent was considered, based on the integral equation formalism model (IEFPCM) (Tomasi et al., 2005). Laplacian bond order (LBO) (Lu and Chen, 2013), energy density of bond critical point (BCP) (Cremer and Kraka, 1984), and atomic dipole corrected Hirshfeld atomic charge (ADCH) were calculated by using the Multiwfn software (Lu and Chen, 2012a). Furthermore, local mode force constant (LMFC) was calculated to evaluate bond strength (Kraka et al., 2020). Multiwfn and VMD software was adopted to analyze and visualize the electron density and electrostatic potential (ESP) of specific molecules (Humphrey et al., 1996; Lu and Chen, 2012b). The value of the molecular ESP minimum was used to probe lone pairs of molecules (Bijina et al., 2018).

In order to examine the variation of toxicities along with the photodegradation of PYM, the LC_{50} and EC_{50} values of PYM and its primary photodegradation products were estimated by using ECOSAR software (US-EPA, 2021).

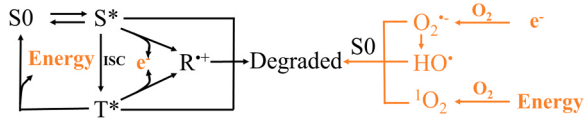

Scheme 1. Potential initiating mechanisms for the photodegradation of PYM in water (Orange part indicates the degradation enhanced by self-sensitization).

3. Results and discussion

3.1. The photodegradation kinetics of PYM on wax surface, in water, and in nonaqueous solvent

Fig. 1a and b shows the photodegradation of the pure PYM reagent (PYM-P), and its commercial formulation (PYM-F) on the surface of paraffin wax, and in water under natural solar light. Control experiments showed that PYM did not degrade in the dark. Eq. (1) indicates that the photodegradation kinetic rate constants of PYM-P and PYM-F are as follows, in descending order: $k'_{water,\ PYM\text{-}P}$ ($1.70 \pm 0.06\ h^{-1}$, r^2 =0.99) > $k'_{water,\ PYM\text{-}F}$ ($0.78 \pm 0.01\ h^{-1}$, r^2 =0.99) >> $k'_{wax,\ PYM\text{-}F}$ ($6.26 \pm 3.33 \times 10^{-3}\ h^{-1}$, r^2 =0.30) ≈ $k'_{wax,\ PYM\text{-}P}$ ($5.50 \pm 1.68 \times 10^{-3}\ h^{-1}$, r^2 =0.62). Wax film is composed of long-chain and saturated aliphatic components, which are efficient hydrogen donators than water (Niu et al., 2003). Therefore, the significantly faster photodegradation of PYM in water was clearly unrelated to the hydrogen abstraction mechanism (Xie et al., 2009). In general, the coexistence of formulates suppressed the photodegradation of PYM in water. This may be attributed to the fact that the formulates competed for the photons or scavenged the reactive species that initiated the photochemical reactions (Sleiman et al., 2017; Peng et al., 2020). The results of the photodegradation of PYM-F indicated that the half-life of PYM was 9.2 days on the surface of paraffin wax, and only 0.9 h in water. This indicates PYM was photostable on leaf surface and photolabile in water.

In order to determine the exact cause of the significant increase in photodegradation kinetics in water, the photodegradation kinetics of PYM was further compared in a homogeneous reaction system containing water, MeOH, and PeOH under xenon lamp (Fig. 1c). The measurements of the photodegradation kinetics of PNA indicate that the irradiance of stimulated sunlight was 4.0 and 5.5 times higher than that of the natural solar light presented in Fig. 1a and b. The absorbance of MeOH and PeOH does not overlap with the emission spectrum of the xenon lamp (emission > 290 nm) (Fig. S1); as such, the light screen and photosensitization due to the solvent could be disregarded. The degradation rate constants in descending order are as follows: k'_{water} ($0.42 \pm 0.04\ h^{-1}$, r^2 =0.95) >> k'_{MeOH} ($2.55 \pm 1.14 \times 10^{-2}\ h^{-1}$, r^2 =0.54) > k'_{PeOH} ($0.72 \pm 0.40 \times 10^{-2}\ h^{-1}$, r^2 =0.55). In accordance with the results observed on wax surface, significantly slow photodegradation was also found in the nonaqueous organic solvents. The results indicate that the physicochemical properties of the solvent significantly enhanced the photodegradation of PYM in water, rather than the interfacial effect and homogeneous dispersion of chemicals. Moreover, slight bathochromic shifts of absorption of PYM were observed in MeOH and PeOH (inset of Fig. 1c). However, the accumulated absorptions of PYM (290–400 nm) in MeOH and PeOH only changed by − 1.98% and 4.65%, which were too small compared to the variations of photodegradation kinetic rates (16.5 times in MeOH and 58.3 times in PeOH). Polar solvent such as water can enhance the photodegradation of organic compounds through the stabilization of ROS such as $^1O_2$ and intermediates such as radical cation ($R^{\bullet+}$) and $O_2^{\bullet-}$ (formed by photoionization, Scheme 1) (Wang et al., 2005). Moreover, the variation of solvents can also change the electronic structure, bond energy and electron donating/accepting activity of organic compounds (Xie et al., 2009).

3.2. Mechanistic investigations on direct photodegradation of PYM

Possibly, that photoinduced processes and reactive species took part into the photodegradation of PYM (Scheme 1). In general, solar light excites the target organic compound to form a singlet excited state (S*), which may further get transformed to a triplet excited state (T *) if intersystem crossing (ISC) occurs (Kaur and Anastasio, 2018). Both S* and T * may directly initiate photodegradation through bond cleavage or isomerization (Di Nunzio et al., 2009). Moreover, S* and T * may interact with molecules in the surrounding environment through electron or energy transfers. The electron transfer may result in direct oxidation and formation of a radical cation ($R^{\bullet+}$), further inducing the subsequent reactions (Shkrob, 2010).

Beyond variations in the structure of the organic compound itself, ROS may also form in the reaction system and engage in the degradation of PYM, representing a self-photosensitization mechanism (Wang et al., 2015). For example, in the electron transfer reaction, the excited-state of the target compound may either draw electrons from reductive compounds to form active radicals (An et al., 2014; Erickson et al., 2015), or transfer electrons to neighboring molecules, mostly dissolved O_2, to form $O_2^{\bullet-}$ (Pajares et al., 2001). The $O_2^{\bullet-}$ may then further transform to oxidative H_2O_2 and $HO^{\bullet}$ through disproportionation (Liu et al., 2015). In the energy transfer reactions, an excited state tends to transfer energy to the adjacent O_2, resulting in the formation of $^1O_2$ (Pan et al., 2018). This results in a selective oxidant that targets unsaturated bonds in organic compounds (Jaramillo et al., 2020).

To further identify the main photoinduced species involved in the photodegradation of PYM, kinetic studies were conducted using different chemical scavengers and probes; and by LFP experiments and the calculation of absorbance spectra for possible transients (T^*_{PYM} and $R^{\bullet+}_{PYM}$). The results are presented in Fig. 2a and b, and Fig. S2. The scavenging of T * by HAD and TMP hardly affected the photodegradation of PYM (Fig. 2a), indicating the photodegradation was not related to T_{PYM}* . O_2 is an efficient scavenger for both T * and hydrated electrons (Buxton et al., 1988; Pan et al., 2018); therefore, the missing transient spectra of T^*_{PYM} (calculated maximum absorption was

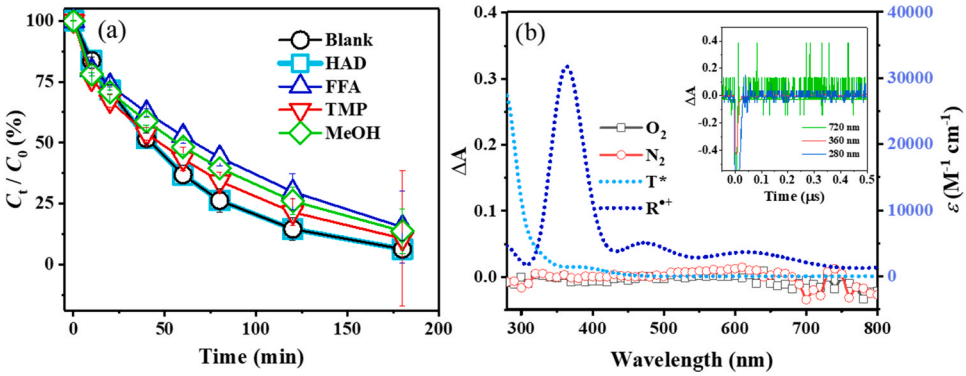

Fig. 2. (a) The photodegradation of 10 μM PYM in solutions with different scavengers (1 mM). (b) The transient spectra corresponding to the left axis were obtained by LFP in O_2 and N_2 saturated water (80 μM PYM at 0.1 μs). The dotted-blue lines correspond to the right axis and indicate the absorption spectra of T^*_{PYM} and $R^{\bullet+}_{PYM}$ calculated at PBE0/def2-TZVPP/IEFPCM level. The inset indicates the evolution of ΔA in N_2-saturated water within 0.5 μs at 720, 360, and 280 nm, corresponding to the absorptions of hydrated electron, T^*_{PYM}, and $R^{\bullet+}_{PYM}$.

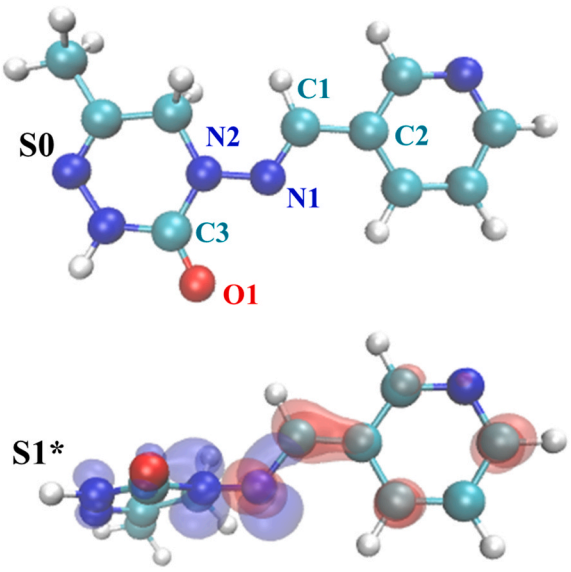

Parameters	S0	S1*
Dihedral angle (°)		
C1N1N2C3	180	-99.87
Bond length (Å)		
C1N1	1.28	1.35
C1C2	1.46	1.4
N1N2	1.36	1.3
Bond order		
C1N1	1.46	1.11
C1C2	1.17	1.44
N1N2	0.75	0.99
Energy density of BCP (a.u.)		
C1N1	-0.57	-0.44
C1C2	-0.25	-0.31
N1N2	-0.34	-0.43
Local force constant (mdyn/Å)		
C1N1	9.51	6.23
C1C2	4.97	6.09
N1N2	5.19	7.11
Atomic charge (a.u.)		
N1	-0.26	-0.48
C1	0.03	0.23
O1	-0.5	-0.51

Fig. 3. Electron excitation analysis visualized based on the hole-electron distribution in S1 $^*_{PYM}$. The bluish-transparent and red-transparent regions indicate where ED decreased and increased, respectively (the ED on the surface was 0.005 electron bohr^{-3}). The data presented in Table summarize the variation in the dihedral angle, bond length, LBO, energy density of BCP, local mode force constant (LMFC) and ADCH atomic charge of specific atom, when PYM was excited from S0 to S1 * (Blue and red color indicate the decrease and increase of the absolute value for specific parameter, respectively).

280 nm) in the N_2-saturated solution with LFP ruled out the occurrence of ISC (Fig. 2b). LFP experiments also revealed the absence of transient signals of hydrated electrons (~720 nm) (Buxton et al., 1988), and no signals of $R^{\bullet+}_{PYM}$ (calculated maximum absorption was ~360 nm) in the N_2-saturated solution. This further supported the non-existence of photoionization. Finally, the absence of $R^{\bullet+}_{PYM}$ in the O_2-saturated solutions further confirmed that one electron oxidation by O_2 (resulting in the formation of $R^{\bullet+}_{PYM}$ and $O_2^{\bullet-}$) did not need to be considered (Fig. S2). These results were consistent with the non-detection of $O_2^{\bullet-}$ using NBT during the photodegradation of PYM (Fig. S3).

The scavenging of $^1O_2$ and $HO^\bullet$ slightly lowered the photodegradation rate, indicating the formation of these two ROSs and their involvement engage in the self-sensitized photodegradation of PYM (Fig. 2a). However, further studies using TPA in the PYM solution found that $HO^\bullet$ was not generated during the photodegradation of PYM (Fig. S3). The degradation of FFA indicates the likely formation of low concentrations of $^1O_2$ (2.42×10^{-14} M) in the 10 μM PYM solution (Fig. S3 and Eq. 1). The $^1O_2$ could further react with PYM at a bimolecular rate constant of 6.63×10^7 M^{-1} s^{-1} (Fang et al., 2020); as such, the part of PYM that was degraded by $^1O_2$ was estimated to be $k'_{1O2} = 1.60 \pm 0.39 \times 10^{-6}$ s^{-1} (Eq. 1). This was a negligible value compared to the observed photodegradation rate constant of PYM in water ($2.63 \pm 0.03 \times 10^{-4}$ s^{-1}, Fig. 2a).

The above-mentioned results indicate that the roles of the long-lived species T_{PYM}* and photosensitized ROSs were negligible in the photodegradation of PYM. The initiating mechanisms could be mostly attributed to S* , which is a short-lived species that is difficult to probe or directly observe by LFP.

3.3. Characterization of the physicochemical properties of S^*_{PYM}

Quantum chemical calculations were performed to study the physicochemical properties of the short-lived S^*_{PYM}. Fig. S4 shows that the calculated UV/Vis spectra of PYM were similar to the measured results. In general, the normalized absorbance from 290 to 400 nm (accumulative absorbance from 290 to 400 nm divided by the absorption at the maximum absorption peak) shifted by 28% for the calculated results. More importantly, the maximum absorption peak exhibited a red shift only by ~4 nm for the calculated spectra. This confirmed the calculation accuracy on estimating the wavelength of maximum peak or photoexcitation energy of PYM at the PBE0/def2-TZVPP level. The calculated energy values of the first, second, and third excited states of S^*_{PYM} (S1 $^*_{PYM}$, S2 $^*_{PYM}$, S3 $^*_{PYM}$) are 4.10 eV (302 nm), 4.58 eV (270 nm), and 4.71 eV (263 nm), respectively. This indicates that only S1 $^*_{PYM}$ is energy-permitted under sunlight photoexciting conditions with wavelengths higher than 290 nm.

S1 $^*_{PYM}$ was optimized at the B3LYP/6–311 +g(d,p)/IEFPCM level in water, and the characteristics of electron excitation were further analyzed based on variation in the electron density (ED). The coordinates of the optimized $S0_{PYM}$ and S1 $^*_{PYM}$ are summarized in Section S1 in Supporting Information, and the calculated results were visualized by using VMD based on the hole–electron distribution as shown in Fig. 3 (Liu et al., 2020). Significant variations in the ED were found in the part (C2C1N1N2) between the two cyclic groups of PYM. In general, the ED between C1 and N1 decreased, indicating a mitigation of the connections between C1 and N1 in S1 $^*_{PYM}$. However, the ED between C1 and C2 significantly increased, indicating possible strengthening of the connections between these two atoms.

Further analysis of the geometric structures of S1 $^*_{PYM}$ and $S0_{PYM}$ showed that the bond length of C1N1 (BL_{C1N1}) increased from 1.28 to 1.35 Å after photoexcitation (Fig. 3). In contrast, BL_{C1C2} decreased from 1.46 to 1.40 Å and BL_{N1N2} decreased from 1.36 to 1.30 Å. The LBO of C1N1 (BO_{C1N1}) decreased from 1.46 to 1.11; that of BO_{C1C2} increased from 1.17 to 1.44; and that of BO_{N1N2} increased from 0.75 to 0.99. Moreover, local mode force constant (LMFC) of C1N1 decreased from 9.51 to 6.23 mdyn Å^{-1}; that of $LMFC_{C1C2}$ increased from 4.97 to 6.09 mdyn Å^{-1}; and that of $LMFC_{N1N2}$ increased from 5.19 to 7.11 mdyn Å^{-1}. These results confirmed that the C1N1 bond (B_{C1N1}) in S1 $^*_{PYM}$ weakened, which was accompanied by the stabilization of B_{C1C2} and B_{N1N2}. Moreover, the absolute values of atomic charges significantly increased in C1 and N1. This indicates the increased possibility of nucleophilic reactions at C1 and electrophilic reactions at N1 when PYM is photoexcited to S1 $^*_{PYM}$ (Liu et al., 2014). Both reactions result from the reorganization of bonding electrons and the formation of new bonds. This then further weakens the connections between C1 and N1, possibly resulting in the bond cleavage.

In summary, the photodegradation of S^*_{PYM} is closely related to the C2C1N1N2 structure in S1 $^*_{PYM}$. The degradation might be initiated by the nucleophilic and electrophilic reactions at the C1 and N1 atoms. This strengthens B_{C1C2} and B_{N1N2}, and weakens B_{C1N1}; causing the potential bond breakage and resulting in the formation of two stable cyclic intermediates. For further comprehensive understanding of the role of C2C1N1N2 in initiating the photodegradation of PYM, six compounds with a similar structure to PYM were also investigated, using quantum

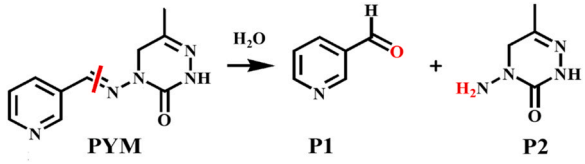

Scheme 2. The main photodegradation pathway of PYM.

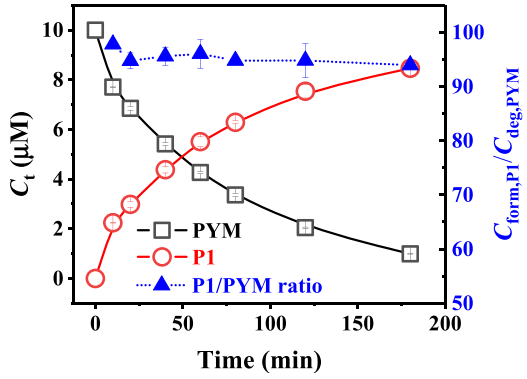

Fig. 4. The evolution of the concentrations of PYM and P1 during the photodegradation of 10 μM PYM in water.

chemical calculations. Variations in electron density, bond order, and atomic charge were compared between $S0_{PYM}$ and S1 $^*_{PYM}$, as summarized in Table S1. The results mostly matched the photodegradation mechanisms, which were assumed to be true for PYM. In general, C1 and N1 charges increased, with the exception of one compound with a terminal $–NH_2$ group. The BO_{C1N1} of five tested compounds decreased, accompanied with a significant increase of BO_{C1C2}. However, BO_{N1N2} decreased in compounds characterized by N2 in a heterocyclic structure. This can happen because of a conjugative effect stabilizing N2 in the cyclic structure, similar to triazine in PYM, rather than in an N–N chain structure (Hu et al., 2001).

3.4. The degradation mechanisms of S1 $^*_{PYM}$ associated with water

In order to further study the degradation mechanisms of S1 $^*_{PYM}$ in water, the photodegradation products were investigated by GC/MS. Only two products were identified, namely, 3-pyridinecarboxaldehyde (P1) and a heterocyclic compound (P2, 4-amino-6-methyl-2H-[1,2,4] triazine-3-one) (Fig. S5, Scheme 2). The mol balance analysis indicated P1 was the main product, contributing 93.9 ± 0.5% of the photodegradation of PYM (Fig. 4). The variations in P2, along with the photodegradation of PYM, were not determined due to the lack of standards. Nevertheless, noteworthy, the sum of the molecular masses for P1 and P2 was equal to the total mass of PYM, two H atoms, and one O atom (Scheme 2). As a result, P2 was considered to be a primary degradation product that was formed simultaneously with P1. The molar concentrations were assumed to be equal if there were no further degradation processes. The results confirmed the theoretical assumption mentioned above: the main degradation pathway of S1 $^*_{PYM}$ was the bond cleavage at C1N1 and the formation of two cyclic products. Noteworthy, the ECOSAR calculations show that P1 and P2 were less toxic than their parent compound PYM (Table S2), indicating the photodegradation of PYM is coupled with detoxification.

The donor of the O atom in P1 could only be attributed to O_2 or H_2O in the reaction system (Scheme 2). O_2 is a well-known nucleophilic reactant, and H_2O can initiate hydrolysis through both nucleophilic and electrophilic reactions (Deng et al., 2008). Notable, O_2 is more soluble in nonpolar solvents such as MeOH and PeOH compared to that in water; therefore, the significantly slow photodegradation of PYM in MeOH and PeOH indicates the reaction between O_2 and PYM would be negligible (Fig. 1c). To further identify the exact reactant with PYM, an isotopic tracing method with H_2O^{18} as the reaction solution was adopted. The isotope ratio for the P1 concentration was measured to be 7.56: 1 ($P1^{110}$: $P1^{108}$) in a H_2O^{18} solution (Fig. S6), which was significantly higher than the value for H_2O^{16} ($P1^{110}$: $P1^{108}$ = 1: 62.05). The results of the isotope labeling showed that the O atom of H_2O engaged in the reactions with S1 $^*_{PYM}$, and the photodegradation mechanism of PYM was a photoinduced hydrolysis process.

The results indicate that H_2O molecules could induce a nucleophilic attack on C1 and an electrophilic attack on N1 in S1 $^*_{PYM}$. Moreover, the triazine ring in $S0_{PYM}$ rotates by 99.87° when photoexcited (Fig. 3); therefore, the molecular torsion shortens the distances between C1 and O1. This led to another possible reaction, where H_2O simultaneously attacked C1 and O1 (Fig. 5a). Further analysis based on the electrostatic potential (ESP) showed that the distance between the lone pairs (ESP minimum) and the nucleus (ESP maximum), N1 and C1, O1 and C1, in S1 $^*_{PYM}$ are 2.25 and 3.16 Å, respectively. These are farther than the distance between lone pairs and protons in H_2O (1.98 Å). The results indicate that one H_2O molecule is not sufficient enough to bridge the gap between both the negative and positive centers of S1 $^*_{PYM}$ to initiate the hydrolysis reactions. Therefore, at least two H_2O molecules are needed for the reaction, with one H_2O molecule acting as the catalyst that transferred the protons as previously observed (Kostko et al., 2016). To test this assumption, the TS for the PYM reaction with one H_2O molecule

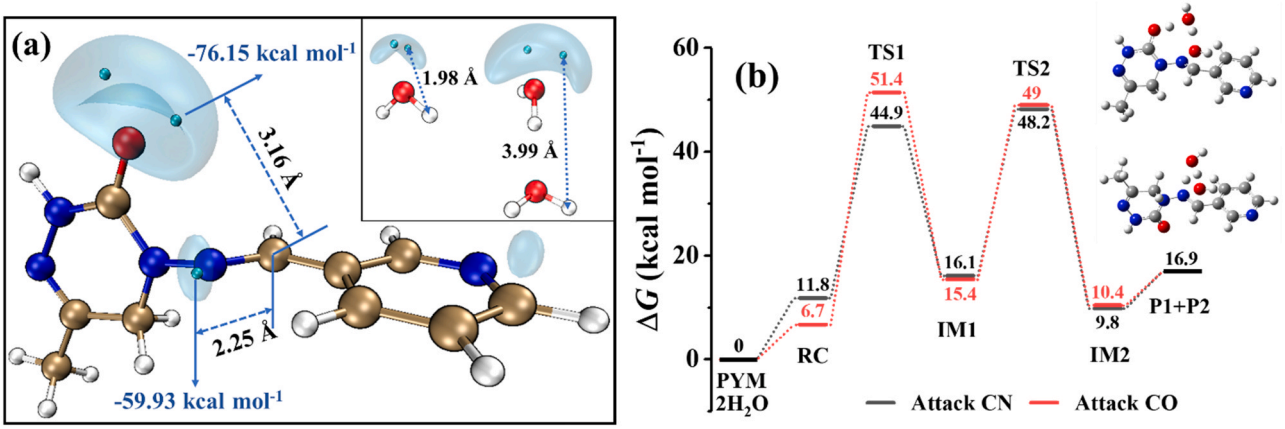

Fig. 5. (a) The negative electrostatic potential (ESP) of S1 $^*_{PYM}$, H_2O, and 2 H_2O (Cyan balls indicate the positions of electrons that correspond to the lowest value of ESP; ESP on isosurface was −55 kcal mol^{-1}). (b) The schematic showing free energy surfaces for the attack of $2H_2O$ on C1N1 and C1O1 (Insets represent the structure of TS1 for each hydrolysis pathway). All calculations were conducted at B3LYP/6–311 +g(d,p)/IEFPCM level.

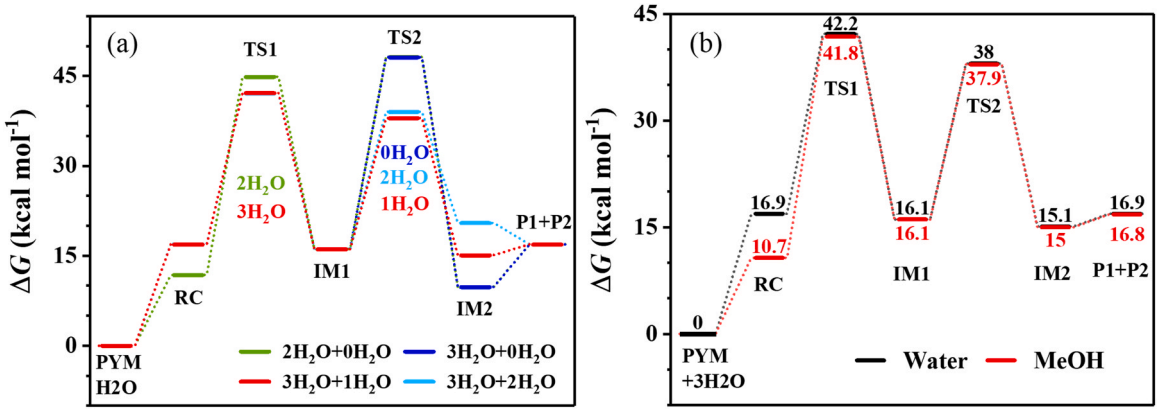

Fig. 6. The schematic showing free energy surfaces for (a) the interaction of PYM with different number of H_2O molecules in water for the two-step reaction, and (b) the photoinduced hydrolysis of PYM in water and in MeOH. All calculations were conducted at B3LYP/6–311 +g(d,p)/IEFPCM level.

was also examined. As expected, no stable structure for TS with only one H_2O was found.

Then, the free energy surfaces for the photoinduced hydrolysis of PYM initiated by two H_2O molecules were established, as shown in Fig. 5b. The geometric structures are presented in Fig. S7 and Section S1. PYM finally degrades to P1 and P2 through a two-step reaction, and the first step is the rate-limiting step due to its higher activation energy barrier (44.9 or 51.4 kcal mol^{-1}) than the second step (32.1 or 33.6 kcal mol^{-1}). The first step (TS1) is the hydrolysis initiated by the direct attack of two H_2O molecules at C1N1 or indirect attack at C1O1. Specifically, the indirect hydrolysis indicates that the –OH of H_2O is added to C1 (the same as direct hydrolysis process), while the H of H_2O is first added to O1, and is then further transferred to N1 (Zhang et al., 2015). The activation energy barrier of direct hydrolysis is more energy-feasible (44.9 kcal mol^{-1}) compared to indirect hydrolysis (51.4 kcal mol^{-1}). The second step (TS2) is the intermolecular hydrogen transfer coupled with the cleavage of B_{C1N1}. Still, the intermediate formed by direct hydrolysis is more energy-feasible (0.8 kcal mol^{-1} lower) than indirect hydrolysis for TS2. The reaction mechanism of TS2 is similar to a keto-enol tautomerism, during which the hydrogen transfer is subsequently followed by the bond dissociation of C1 and N1 (Mallick et al., 2007). Analysis of the free energy surfaces shows that an H_2O attack on C1N1 is more energy favorable than on C1O1 for both TS1 and TS2. Furthermore, the role of C2C1N1N2 in initiating the photoinduced hydrolysis was also examined for the similar compounds list in Table S1. The activation energy barriers (TS1) of these six compounds were in the range of 30.6–40.7 kcal mol^{-1} (Table S3), which were comparable to that of PYM, probably indicating hydrolysis is a common mechanism for the reaction of C2C1N1N2.

3.5. Other physicochemical effects of water on the photoinduced hydrolysis of PYM

Besides a direct chemical reaction, water may also affect the photoinduced hydrolysis of PYM through two other possible mechanisms. First, the H_2O molecule was confirmed to be the catalyst for proton transfer. It was assumed that the number of H_2O molecules could also influence the activation energy barrier, and the reaction rate constant (Deng et al., 2008). Second, as a high polarity solvent, water could affect the ESP, bond energy, and atomic charges of organic compounds. These could ultimately result in the variation of photodegradation kinetics (Pan et al., 2016). Therefore, the catalytic activity and solvent effect of H_2O on the free energy surfaces of the photoinduced hydrolysis of PYM were further calculated, as shown in Fig. 6a and b. The geometric structures of key TS and the reaction pathways are presented in Fig. 7 and Section S1.

Results show that the activation energy barrier for hydrolysis (TS1) was lowered (−2.44 kcal mol^{-1}) when an additional H_2O molecule was added as the catalyst (three in total). The activation energy barrier for the intramolecular hydrogen transfer (TS2) is as follows: zero H_2O molecule (32.04 kcal mol^{-1}) > two H_2O molecules (22.93 kcal mol^{-1}) > one H_2O molecule (21.91 kcal mol^{-1}). The results indicate that water molecules show catalytic effects during both the reaction steps. A more significant catalytic effect was observed for TS2. H_2O plays an important role as the catalyst in the keto-enol tautomerism in the TS2 setting (Kouras-Hadef et al., 2011). However, changing the solvent from MeOH to water increased the activation energy barriers of TS1 and TS2 by 0.38 and 0.12 kcal mol^{-1}, respectively (Fig. 6b). This indicates a slightly negative solvent effect of water on PYM photodegradation. Therefore, these results suggest solvent effect can be disregarded compared to the chemical reactions and catalytic effects introduced by water molecules.

4. Conclusions

The photodegradation of PYM is significantly faster in water compared to the leaf and nonaqueous solutions. The photodegradation is mainly initiated by S1 $^*_{PYM}$. Along with the photoexcitation, B_{C1N1} was weakened, and photoinduced hydrolysis occurred in C1N1 as the first step of photodegradation. The second reaction step of photodegradation involved the intramolecular hydrogen transfer in the intermediate formed during first step, coupled with the cleavage of B_{C1N1}. This resulted in the breakage of the intermediate, and formation of two stable cyclic products. During both the reaction steps, water molecules show a strongly catalytic effect by acting as bridges between negative and positive centers of PYM and its intermediate, and the solvent effect of water is negligible.

CRediT authorship contribution statement

Ximei Liang: Methodology, Data curation, Writing – original draft, Writing - review & editing, Funding acquisition. **Fangling Guan:** Investigation, Data curation, Writing – original draft. **Zhiyou Ling:** Investigation, Resources. **Honghong Wang:** Methodology, Resources. **Yunwen Tao:** Software, Writing – review & editing. **Elfi Kraka:** Software, Writing – review & editing. **Huanjun Huang:** Resources, Validation. **Chenglong Yu:** Formal analysis. **Danping Li:** Formal analysis. **Jinbao He:** Validation. **Hansun Fang:** Conceptualization, Writing – review & editing, Supervision, Project administration, Funding acquisition.

Declaration of Competing Interest

The authors declare that they have no known competing financial interests or personal relationships that could have appeared to influence

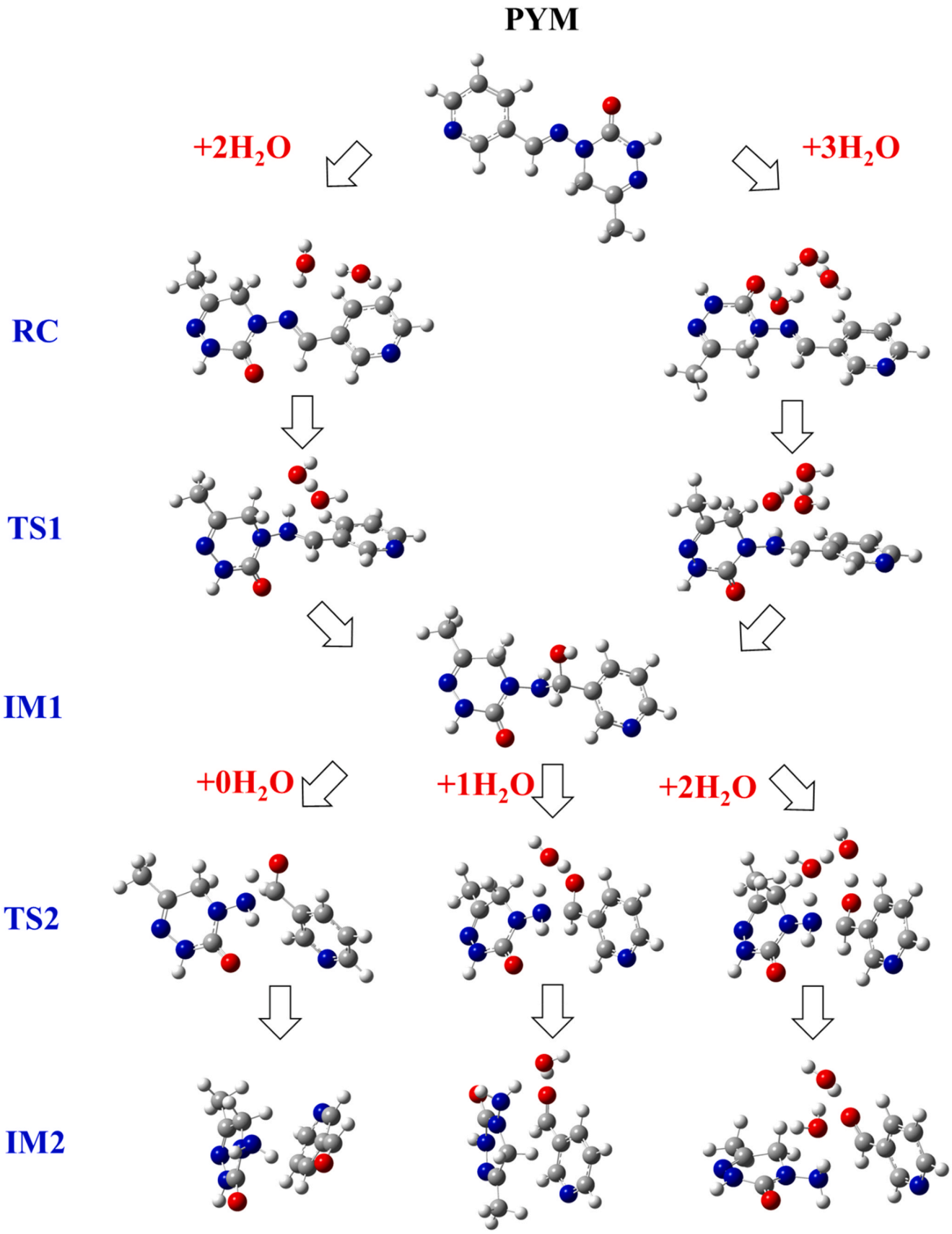

Fig. 7. Stationary points for the photoinduced hydrolysis of PYM considering the catalytic effects by different number of H_2O molecules (calculated at B3LYP/6–311 +g(d,p)/IEFPCM level).

the work reported in this paper.

Acknowledgment

The authors greatly acknowledge the financial support from the National Natural Science Foundation of China (Grant no. 21607065), the Natural Science Foundation of Jiangxi Province, China (Grant no. 20202BABL205006) and the Special Innovation Fund for Graduate Students of Jiangxi Province, China (YC2019-S179). The authors are also thankful to Professor Taicheng An and Dr. Na Luo for their kind help in conducting laser experiments and for useful discussions. Y. Tao and E. Kraka are thankful to SMU for providing supercomputing resources.

Appendix A. Supporting information

Supplementary data associated with this article can be found in the online version at doi:10.1016/j.jhazmat.2021.127197.

References

An, T., Fang, H., Li, G., Wang, S., Yao, S., 2014. Experimental and theoretical insights into photochemical transformation kinetics and mechanisms of aqueous propylparaben and risk assessment of its degradation products. Environ. Toxicol. Chem. 33, 1809–1816.

Andersson, M.P., Uvdal, P., 2005. New scale factors for harmonic vibrational frequencies using the B3LYP density functional method with the triple-ζbasis set 6-311+G(d,p). J. Phys. Chem. A 109, 2937–2941.

Anglada, J.M., Martins-Costa, M.T.C., Francisco, J.S., Ruiz-Lopez, M.F., 2020. Photoinduced oxidation reactions at the air-water interface. J. Am. Chem. Soc. 142, 16140–16155.

Becke, A.D., 1993. Density-functional thermochemistry. III. The role of exact exchange. J. Chem. Phys. 98, 5648–5652.

Bijina, P.V., Suresh, C.H., Gadre, S.R., 2018. Electrostatics for probing lone pairs and their interactions. J. Comput. Chem. 39, 488–499.

Broughton, S., Harrison, J., Rahman, T., 2014. Effect of new and old pesticides on Orius armatus (Gross) - an Australian predator of western flower thrips, Frankliniella occidentalis (Pergande). Pest Manag. Sci. 70, 389–397.

Buxton, G.V., Greenstock, C.L., Helman, W.P., Ross, A.B., 1988. Critical-review of rate constants for reactions of hydrated electrons, hydrogen-atoms and hydroxyl radicals (.OH/.O-) in aqueous-solution. J. Phys. Chem. Ref. Data 17, 513–886.

Cabizza, M., Satta, M., Falconi, S., Onano, M., Uccheddu, G., 2007. Degradation of cyprodinil, fludioxonil, cyfluthrin and pymetrozine on lettuce after different application methods. J. Environ. Sci. Heal. B. 42, 761–766.

Casado, J., Brigden, K., Santillo, D., Johnston, P., 2019. Screening of pesticides and veterinary drugs in small streams in the European Union by liquid chromatography high resolution mass spectrometry. Sci. Total Environ. 670, 1204–1225.

Cremer, D., Kraka, E., 1984. Chemical bonds without bonding electron density-Does the difference electron-density analysis suffice for a description of the chemical bond? Angew. Chem. Int. Ed. Engl. 23, 627–682.

De Souza, R.M., Seibert, D., Quesada, H.B., Bassetti, F.D., Fagundes-Klen, M.R., Bergamasco, R., 2020. Occurrence, impacts and general aspects of pesticides in surface water: a review. Process Saf. Environ. Prot. 135, 22–37.

Deng, C., Li, Q.G., Ren, Y., Wong, N.B., Chu, S.Y., Zhu, H.J., 2008. A comprehensive theoretical study on the hydrolysis of carbonyl sulfide in the neutral water. J. Comput. Chem. 29, 466–480.

Di Nunzio, M.R., Romani, A., Favaro, G., 2009. Excited-state properties of a photochromic spirooxazine: double pathways for both fluorescence emission and camphorquinone-sensitized reaction. J. Phys. Chem. A 113, 9424–9433.

Dulin, D., Mill, T., 1982. Development and evaluation of sunlight actinometers. Environ. Sci. Technol. 16, 815–820.

Ebrahimi, P., Spooner, J., Weinberg, N., Plettner, E., 2013. Partition, sorption and structure activity relation study of dialkoxybenzenes that modulate insect behavior. Chemosphere 93, 54–60.

Elfikrie, N., Ho, Y.B., Zaidon, S.Z., Juahir, H., Tan, E.S.S., 2020. Occurrence of pesticides in surface water, pesticides removal efficiency in drinking water treatment plant and potential health risk to consumers in Tengi River Basin, Malaysia. Sci. Total Environ. 712, 136540.

Erickson, P.R., Walpen, N., Guerard, J.J., Eustis, S.N., Arey, J.S., McNeill, K., 2015. Controlling factors in the rates of oxidation of anilines and phenols by triplet methylene blue in aqueous solution. J. Phys. Chem. A 119, 3233–3243.

Fang, H., Ling, Z., Guan, F., Liao, W., Lai, F., Liang, X., 2020. Photophysical and photochemical insights into the photodegradation of tricyclazole and pymetrozine in water bodies of a rice field. Environ. Chem. 17, 436–444.

Fenner, K., Canonica, S., Wackett, L.P., Elsner, M., 2013. Evaluating pesticide degradation in the environment: blind spots and emerging opportunities. Science 341, 752–758.

Frisch, M.J., Trucks, G.W., Schlegel, H.B., Scuseria, G.E., Robb, M.A., Cheeseman, J.R., Scalmani, G., Barone, V., Petersson, G.A., Nakatsuji, H., Li, X., Caricato, M., Marenich, A.V., Bloino, J., Janesko, B.G., Gomperts, R., Mennucci, B., Hratchian, H. P., Ortiz, J.V., Izmaylov, A.F., Sonnenberg, J.L., Williams-Young, D., Ding, F., Lipparini, F., Egidi, F., Goings, J., Peng, B., Petrone, A., Henderson, T., Ranasinghe, D., Zakrzewski, V.G., Gao, J., Rega, N., Zheng, G., Liang, W., Hada, M., Ehara, M., Toyota, K., Fukuda, R., Hasegawa, J., Ishida, M., Nakajima, T., Honda, Y., Kitao, O., Nakai, H., Vreven, T., Throssell, K., Montgomery, J.A., Peralta Jr., J.E., Ogliaro, F., Bearpark, M.J., Heyd, J.J., Brothers, E.N., Kudin, K.N., Staroverov, V.N., Keith, T.A., Kobayashi, R., Normand, J., Raghavachari, K., Rendell, A.P., Burant, J. C., Iyengar, S.S., Tomasi, J., Cossi, M., Millam, J.M., Klene, M., Adamo, C., Cammi, R., Ochterski, J.W., Martin, R.L., Morokuma, K., Farkas, O., Foresman, J.B., Fox, D.J., 2016. Gaussian 16, Revision A.03. Gaussian, Inc., Wallingford CT.

Hu, C., Wang, Y.Z., Tang, H.X., 2001. Influence of adsorption on the photodegradation of various dyes using surface bond-conjugated TiO2/SiO2 photocatalyst. Appl. Catal. B Environ. 35, 95–105.

Humphrey, W., Dalke, A., Schulten, K., 1996. VMD: Visual molecular dynamics. J. Mol. Graph. 14, 33–38.

Jaramillo, M., Joens, J.A., O'Shea, K.E., 2020. Fundamental studies of the singlet oxygen reactions with the potent marine toxin domoic acid. Environ. Sci. Technol. 54, 6073–6081.

Jia, G., Zeng, L., Zhao, S., Ge, S., Long, X., Zhang, Y., Hu, D., 2019. Monitoring residue levels and dietary risk assessment of pymetrozine for Chinese consumption of cauliflower. Biomed. Chromatogr. 33, e4455.

Kah, M., Navarro, D., Kookana, R.S., Kirby, J.K., Santra, S., Ozcan, A., Kabiri, S., 2019. Impact of (nano) formulations on the distribution and wash-off of copper pesticides and fertilisers applied on citrus leaves. Environ. Chem. 16, 401–410.

Kaur, R., Anastasio, C., 2018. First measurements of organic triplet excited states in atmospheric waters. Environ. Sci. Technol. 52, 5218–5226.

Kim, K.H., Kabir, E., Jahan, S.A., 2017. Exposure to pesticides and the associated human health effects. Sci. Total Environ. 575, 525–535.

Kostko, O., Troy, T.P., Bandyopadhyay, B., Ahmed, M., 2016. Proton transfer in acetaldehyde-water clusters mediated by a single water molecule. Phys. Chem. Chem. Phys. 18, 25569–25573.

Kouras-Hadef, S., de Sainte-Claire, P., ter Halle, A., Amine-Khodja, A., Richard, C., 2011. The role of triplet state keto-enol tautomerism in the photodeamination of metamitron. J. Phys. Chem. A 115, 14397–14406.

Kraka, E., Zou, W., Tao, Y., 2020. Decoding chemical information from vibrational spectroscopy data: Local vibrational mode theory. WiRes Comput. Mol. Sci. 10, e1480.

Kuang, L.H., Hou, Y.Z., Huang, F.Q., Hong, H.C., Sun, H.J., Deng, W.J., Lin, H.J., 2020. Pesticide residues in breast milkand the associated risk assessment: A review focused on China. Sci. Total Environ. 727, 138412.

Lee, C., Yang, W., Parr, R.G., 1988. Development of the Colle-Salvetti correlation-energy formula into a functional of the electron density. Phys. Rev. B 98, 785–789.

Lei, Y., Cheng, S., Luo, N., Yang, X., An, T., 2019. Rate constants and mechanisms of the reactions of Cl• and Cl2•− with trace organic contaminants. Environ. Sci. Technol. 53, 11170–11182.

Li, C., Yang, T., Huangfu, W., Wu, Y., 2011. Residues and dynamics of pymetrozine in rice field ecosystem. Chemosphere 82, 901–904.

Liu, S., Rong, C., Lu, T., 2014. Information conservation principle determines electrophilicity, nucleophilicity, and regioselectivity. J. Phys. Chem. A 118, 3698–3704.

Liu, W., Liu, H.C., Ai, Z.H., 2015. In-situ generated H_2O_2 induced efficient visible light photo-electrochemical catalytic oxidation of PCP-Na with TiO_2. J. Hazard. Mater. 288, 97–103.

Liu, Z., Lu, T., Chen, Q., 2020. An sp-hybridized all-carboatomic ring, cyclo[18]carbon: electronic structure, electronic spectrum, and optical nonlinearity. Carbon 165, 461–467.

Lu, T., Chen, F., 2012a. Atomic dipole moment corrected Hirshfeld population method. J. Theor. Comput. Chem. 11, 163–183.

Lu, T., Chen, F., 2012b. Multiwfn: a multifunctional wavefunction analyzer. Comput. Chem. 33, 580–592.

Lu, T., Chen, F., 2013. Bond order analysis based on the Laplacian of electron density in fuzzy overlap space. J. Phys. Chem. A 117, 3100–3108.

Mallick, A., Purkayastha, P., Chattopadhyay, N., 2007. Photoprocesses of excited molecules in confined liquid environments: an overview. J. Photochem. Photobiol. C Photochem. Rev. 8, 109–127.

Monadjemi, S., El Roz, M., Richard, C., Ter Halle, A., 2011. Photoreduction of chlorothalonil fungicide on plant leaf models. Environ. Sci. Technol. 45, 9582–9589.

Münze, R., Orlinskiy, P., Gunold, R., Paschke, A., Kaske, O., Beketov, M.A., Hundt, M., Bauer, C., Schüürmann, G., Möder, M., Liess, M., 2015. Pesticide impact on aquatic invertebrates identified with Chemcatcher® passive samplers and the SPEARpesticides index. Sci. Total Environ. 537, 69–80.

National Bureau of Statistics of China, 2020. ⟨http://www.stats.gov.cn/tjsj/⟩ (available in July, 2021).

Niu, J., Chen, J., Henkelmann, B., Quan, X., Yang, F., Kettrup, A., Schramm, K.W., 2003. Photodegradation of PCDD/Fs adsorbed on spruce (*Picea abies (L.) Karst.*) needles under sunlight irradiation. Chemosphere 50, 1217–1225.

Pajares, A., Gianotti, J., Stettler, G., Bertolotti, S., Criado, S., Posadaz, A., Amat-Guerri, F., Garcia, N.A., 2001. Modelling the natural photodegradation of water contaminants - A kinetic study on the light-induced aerobic interactions between riboflavin and 4-hydroxypyridine. J. Photoch. Photobio. A 139, 199–204.

Pan, Y., Tsang, D.C.W., Wang, Y., Li, Y., Yang, X., 2016. The photodegradation of polybrominated diphenyl ethers (PBDEs) in various environmental matrices: kinetics and mechanisms. Chem. Eng. J. 297, 74–96.

Pan, Y., Garg, S., Waite, T.D., Yang, X., 2018. Copper inhibition of triplet-induced reactions involving natural organic matter. Environ. Sci. Technol. 52, 2742–2750.

Peng, R.F., Pang, Y.X., Qiu, X.Q., Qian, Y., Zhou, M.S., 2020. Synthesis of anti-photolysis lignin-based dispersant and its application in pesticide suspension concentrate. RSC Adv. 10, 13830–13837.
Perez-Rodriguez, P., Soto-Gomez, D., Paradelo, M., Lopez-Periago, J.E., 2017. Concentration levels of new-generation fungicides in throughfall released by foliar, wash-off from vineyards. J. Environ. Manag. 203, 467–475.
Preetha, G., Stanley, J., Suresh, S., Samiyappan, R., 2010.). Risk assessment of insecticides used in rice on miridbug, *Cyrtorhinus lividipennis Reuter*, the important predator of brown planthopper, *Nilaparvata lugens* (*Stal.*). Chemosphere 80, 498–503.
Satpathy, S., Gotyal, B.S., Babu, V.R., 2020. Role of novel insecticides in crop protection and their selectivity to natural enemies: a review. J. Environ. Biol. 41, 149–160.
Sharma, A., Kumar, V., Shahzad, B., Tanveer, M., Sidhu, G.P.S., Handa, N., Kohli, S.K., Yadav, P., Bali, A.S., Parihar, R.D., 2019. Worldwide pesticide usage and its impacts on ecosystem. SN Appl. Sci. 1, 1446.
Shen, G., Hu, X., Hu, Y., 2009. Kinetic study of the degradation of the insecticide pymetrozine in a vegetable-field ecosystem. J. Hazard. Mater. 164, 497–501.
Shkrob, I.A., 2010. Deprotonation and oligomerization in photo-, radiolytically, and electrochemically induced redox reactions in hydrophobic alkylalkylimidazolium ionic liquids. J. Phys. Chem. B 114, 368–375.
Sleiman, M., de Sainte Claire, P., Richard, C., 2017. Heterogeneous photochemistry of agrochemicals at the leaf surface: a case study of plant activator acibenzolar-s-methyl. J. Agric. Food Chem. 65, 7653–7660.
Slieman, T.A., Nicholson, W.L., 2000. Artificial and solar UV radiation induces strand breaks and cyclobutane pyrimidine dimers in Bacillus subtilis spore DNA. Appl. Environ. Microbiol. 66, 199–205.
Theitler, D.J., Nasser, A., Gerchman, Y., Kribus, A., Mamane, H., 2012. Synergistic effect of heat and solar UV on DNA damage and water disinfection of *E. coli* and bacteriophage MS2. J. Water Heal. 10, 605–618.
Tomasi, J., Mennucci, B., Cammi, R., 2005. Quantum mechanical continuum solvation models. Chem. Rev. 105, 2999–3093.
US-EPA (United States Environmental Protection Agency). EPI Suite 4.1. ⟨https://www.epa.gov/tsca-screening-tools/epi-suitetm-estimation-program-interface⟩ (available in July, 2021).
Walker, M.K., Stufkens, M.A.W., Wallace, A.R., 2007. Indirect non-target effects of insecticides on Tasmanian brown lacewing (Micromus tasmaniae) from feeding on lettuce aphid (Nasonovia ribisnigri). Biol. Control. 43, 31–40.
Wang, D., Chen, J., Xu, Z., Qiao, X., Huang, L., 2005. Disappearance of polycyclic aromatic hydrocarbons sorbed on surfaces of pine [*Pinua thunbergii*] needles under irradiation of sunlight: Volatilization and photolysis. Atmos. Environ. 39, 4583–4591.
Wang, X., Hu, X., Zhang, H., Chang, F., Luo, Y., 2015. Photolysis kinetics, mechanisms, and pathways of tetrabromobisphenol a in water under simulated solar light irradiation. Environ. Sci. Technol. 49, 6683–6690.
Xie, Q., Chen, J., Shao, J., Chen, C. e, Zhao, H., Hao, C., 2009. Important role of reaction field in photodegradation of deca-bromodiphenyl ether: theoretical and experimental investigations of solvent effects. Chemosphere 76, 1486–1490.
Yu, J.X., Xu, E.G., Li, W., Jin, S.Y., Yuan, T., Liu, J.S., Li, Z.J., Zhang, T.L., 2018. Acute toxicity of an emerging insecticide pymetrozine to Procambarus clarkii associated with rice-crayfish culture (RCIS). Int. J. Environ. Res. Public Health 15, 984.
Zeng, T., Arnold, W.A., 2013. Pesticide photolysis in prairie potholes: probing photosensitized processes. Environ. Sci. Technol. 47, 6735–6745.
Zhang, H., Xie, H., Chen, J., Zhang, S., 2015. Prediction of hydrolysis pathways and kinetics for antibiotics under environmental pH conditions: a quantum chemical study on cephradine. Environ. Sci. Technol. 49, 1552–1558.
Zhang, W., 2018. Global pesticide use: Profile, trend, cost/benefit and more. Proc. Int. Acad. Ecol. Environ. Sci. 8, 1.
Zhang, X., Cheng, X., Wang, C., Xi, Z., Li, Q., 2007. Efficient high-performance liquid chromatography with liquid-liquid partition cleanup method for the determination of pymetrozine in tobacco. Anal. Chim. 97, 295–301.